J. Fluid Mech. (2001), *vol.* 446, *pp.* 1–24.
DOI: 10.1017/S0022112001005626 Printed in the United Kingdom

Self-similar states in turbulent mixing layers

By ELIAS BALARAS, UGO PIOMELLI AND JAMES M. WALLACE

Department of Mechanical Engineering, University of Maryland, College Park, MD 20742, USA

(Received 14 March 2000 and in revised form 3 May 2001)

Large-eddy simulations of temporally evolving turbulent mixing layers have been carried out. The effect of the initial conditions and the size of the computational box on the turbulent statistics and structures is examined in detail. A series of calculations was initialized using two different realizations of a spatially developing turbulent boundary-layer with their free streams moving in opposite directions. Computations initialized with mean flow plus random perturbations with prescribed moments were also conducted. In all cases, the initial transitional stage, from boundary-layer turbulence or random noise to mixing-layer turbulence, was followed by a self-similar period. The self-similar periods, however, differed considerably: the growth rates and turbulence intensities showed differences, and were affected both by the initial condition and by the computational domain size. In all simulations the presence of quasi-two-dimensional spanwise rollers was clear, together with 'braid' regions with quasi-streamwise vortices. The development of these structures, however, was different: if strong rollers were formed early (as in the cases initialized by random noise), a well-organized pattern persisted throughout the self-similar period. The presence of boundary layer turbulence, on the other hand, inhibited the growth of the inviscid instability, and delayed the formation of the roller–braid patterns. Increasing the domain size tended to make the flow more three-dimensional.

1. Introduction

Mixing layers that form between two fluid streams moving with different velocities have been studied both in experiments and simulations for about sixty years. These studies cover a wide range of Reynolds numbers, velocity ratios, and upstream conditions. The motivation behind this continuous effort is not only the technological importance of these flows, but also the rather large disparity in the results obtained in what was initially thought to be a fairly simple flow with a predictable asymptotic behaviour. Determination of the asymptotic behaviour of the mean flow was first attempted by Kuethe (1935), using Prandtl's mixing length to model the Reynolds shear stress term in the boundary layer equations that approximately describe this flow. A solution that better fits the single-stream mixing layer experimental data of Reichardt (1942) was found by Görtler (1942) using Prandtl's constant eddy viscosity hypothesis. They, and many others, have shown that for sufficiently high Reynolds numbers, the equations governing the development of a plane mixing layer can yield 'self-similar' solutions. Self-similarity is characterized by linear growth of the layer, and mean velocities and turbulent statistics that are independent of the downstream distance when normalized by appropriate length and velocity scales. Another characteristic of mixing layers is the presence of large-scale organized structures, whose size is

comparable with the transverse length scale of the flow. Although explicit recognition of the presence and role of organized structures in turbulent flows was apparent earlier (see Cantwell 1981 for a review), it was the Brown & Roshko (1974) flow visualizations that dramatically showed the presence of apparently two-dimensional structures in turbulent mixing layers. Since then, a large number of studies directed toward determining the origin and dynamical significance of coherent structures in mixing layers has been conducted.

Despite the progress made, however, several areas of confusion still remain. There is a large variation in the results among the different experimental studies (see Brown & Roshko 1974 and Dimotakis 1991 for summaries of the experimental results), even when the parameters of the mean flow, including the velocity ratios, are nominally the same. Dimotakis & Brown (1976) suggested that this variation is due to different upstream conditions, namely whether or not the boundary layers at the trailing edge of the splitter plate are laminar or turbulent. For laminar and turbulent initial conditions, given sufficient downstream distance, the layer will become self-similar. In the former case, however, this state is preceded by transition from laminar to turbulent flow (mixing transition); in the latter, transition from boundary-layer turbulence to mixing-layer turbulence occurs before self-similarity. In an experimental study of a single-stream mixing layer, Bradshaw (1966) showed that the asymptotic growth rate for the case with a turbulent boundary layer is higher than for a laminar one. Later experiments performed by Batt (1975) and Hussain & Zedan (1978) confirmed this result. Moreover, in Batt's experiment the growth rates reported in the experiments of Liepmann & Laufer (1947) (laminar boundary layer) and Wygnanski & Fiedler (1970) (turbulent boundary layer), which differed by 30%, could be reproduced by tripping or not tripping the boundary layer in the same apparatus.

In two-stream mixing layers, upstream conditions were also found to affect the results. Contrary to single-stream experiments, however, the asymptotic growth rates were higher when the boundary layers at the end of the splitter plate were laminar, than when they were turbulent (see for example, Browand & Latigo 1979; Metha & Westphal 1986; Bell & Metha 1990). In the Bell & Mehta (1990) experiment the measured growth rates for the tripped and untripped cases differed by 25%, while mean velocities and turbulent quantities were found to collapse within 10% when plotted in similarity coordinates. However, the peak of the secondary shear stress (streamwise–spanwise component), which can be associated with the presence of streamwise rib vortices, was found to decay slowly for the untripped case. This indicated that, although self-similarity was achieved for most quantities, the detailed flow structure could be different. This is also supported by the experimental results of Slessor, Bond & Dimotakis (1998). They studied the effect of initial conditions in two-stream turbulent mixing layers by tripping one or both boundary layers on the splitter plate. It was found that both the mixing layer growth and the molecular mixing, phenomena associated with the large- and small-scale structure respectively, were affected by the upstream conditions. Their colour schlieren visualizations, although obscuring the local structures due to the optical integration in the spanwise direction, indicate a clear decrease in the two-dimensional organization of the flow in the tripped case.

The experimental studies mentioned above point to the possibility that mixing layers may achieve asymptotic self-preserving states that are not independent of their initial conditions, and thus are not unique. A similar behaviour has been observed in other free-shear flows as well. Wygnanski, Champagne & Marasli (1986) for example, reported very different growth rates for wakes behind a cylinder, an airfoil and a screen, all with the same drag coefficient (and thus momentum thickness) and aspect

ratio. All these wakes appeared to be self-preserving. A theoretical explanation for this finding was given by George (1989). He applied similarity analysis to the equations governing the mean flow and Reynolds stresses for the case of a plane jet and showed that, for sufficiently high Reynolds numbers, self-similar solutions were possible for all turbulent quantities. The asymptotic power-law behaviour obtained for the Reynolds stresses, however, was found to depend on the initial state of the source of the jet.

The exact mechanisms producing such differences and the role of coherent structures in this process are not well understood. For laminar boundary layer initial conditions it is known that two-dimensional rollers form that are unstable to sub-harmonic disturbances, leading to pairing (see Ho & Huerre 1984 for a review). These initially two-dimensional rollers are also unstable to three-dimensional disturbances that result in their bending and in the concurrent formation of rib vortices in the 'braid' regions between the rollers (e.g. in Lasheras & Choi 1988 and Rogers & Moser 1992). Spanwise rollers have also been observed in the later stage turbulent region of the mixing layer, where they coexist with a fine-scale motion. These structures are evident in several experimental studies for a wide range of Reynolds numbers (e.g. in Dimotakis & Brown 1976 and Hussain & Zaman 1985). Their dynamics appear to be similar to those of their laminar counterparts, although there is some uncertainty related to the pairing mechanism and the formation of rib vortices.

In addition to the initial conditions, in experimental studies the apparatus can have a significant influence on the results. Large-scale acoustic or pressure feedback effects can change the evolution of the flow. Dziomba & Fiedler (1985) suggested that even very weak perturbations caused by the apparatus may result in significant differences in the spreading rate. They also found that this effect is larger when the boundary layers on the splitter plate are turbulent. Sidewall effects can also be considerable. Hussain (1980) suggested that spanwise coherence of rollers in some experiments could be due to organization by sidewalls. Weisbrot, Einav & Wygnanski (1982) found that even for mixing layers with the same velocity ratio and initialized with laminar boundary layers, the growth rate in the self-similar region varied significantly depending on the absolute level of the free-stream velocities. They attribute this to a Strouhal number effect arising from frequencies inherent in the facility. Oster & Wygnanski (1982) found that a unique self-similar state was never attained for the two-stream mixing layers with forced, very low-amplitude perturbations at the splitter plate.

Numerical simulations, which can be conducted in an accurately controlled environment, are a valuable tool in addressing some of the issues raised above. Simulations are free from various uncontrollable parameters which make the interpretation of different experiments difficult, and can be complementary to currently available experimental results. They can also provide detailed quantitative information on the evolution and dynamics of coherent structures. To avoid the difficulties associated with the imposition of the inflow condition and the computational expense due to the significant length required to develop self-similar states, most numerical simulations of mixing-layer flows performed to date have been temporal simulations. Periodic boundary conditions are applied in the streamwise and spanwise directions, and the flow is allowed to develop in time. If Taylor's hypothesis holds, one can then relate time to space through a Galilean transformation with an appropriate convection velocity. In most of these temporal simulations the base flow was assumed to be a hyperbolic tangent profile, with superimposed two- or three-dimensional disturbances. Several simulations of this type, which resemble experiments with laminar incoming boundary layers, have been reported in the literature (see, for instance, Riley & Metcalfe 1980; Vreman, Geurts & Kuerten 1997; Comte, Silvestrini & Bégou 1998).

These studies gave valuable quantitative information on the fundamental mechanisms underlying the formation and dynamics of coherent structures and their effect on turbulent statistics in transitional mixing layers.

There are fewer simulation studies where the boundary layers on the splitter plate are turbulent, on the other hand. Rogers & Moser (1994) performed a temporal direct numerical simulation (DNS) starting from two different realizations of a turbulent boundary layer with their free streams moving in opposite directions. In their computation, which has many characteristics resembling experiments with incoming turbulent boundary layers, the flow also became self-similar after an initial transient. Statistical properties of the simulated velocity field during self-similarity agreed well with experiments at similar Reynolds numbers. While their results suggest that there may be alternating or non-unique self-similar states, they do not indicate whether such states are temporary or persist indefinitely, because of the limited time evolution of the flow in a limited computational domain. Given the cost of DNS further integration in time on a larger computational box would be prohibitively expensive.

The objective of the present study is to complement the numerical simulations of Rogers & Moser (1994) and the experimental work on the effect of initial conditions on turbulent mixing layers (e.g. Slessor *et al.* 1998), by providing both quantitative and qualitative information on the development of the self-similar states, and on the influence of initial and boundary conditions on this development. Compared with the DNS, the present large-eddy simulation (LES) investigation can explore a larger range of parameters, given the reduced cost of such computations. Compared with experiments, we are able to visualize the turbulent eddies in greater detail, compared with the smoke visualization or schlieren methods used in the literature. First, we will clarify the findings of the DNS by Rogers & Moser (1994) above, regarding the uniqueness or not of the self-similar states of unforced mixing layers, by removing the ambiguity introduced by the limited extent of the computational box in the streamwise and spanwise directions. Having established that, we will focus on the effect of the initial conditions on the evolution of the layer. This type of study can be complementary to existing experimental and DNS studies, and, in addition to flow statistics, it can provide accurate quantitative information on the role and dynamics of coherent structures in the establishment of self-similar states for different upstream conditions.

For this purpose several calculations were carried out using different initial conditions and computational domains, the largest one being four times the size of that employed in the DNS of Rogers & Moser (1994). A parametric study of this sort using DNS would be prohibitively expensive, given the size of the computational domain. The LES approach is an accurate tool to study the dynamics of free shear layers (see, for instance, Ghosal & Rogers 1997; Vreman *et al.* 1997; Comte *et al.* 1998), particularly if small-scale information is not required. The large scales are resolved directly like in a DNS, while the small scales are modelled through a subgrid-scale (SGS) model. However, although LES gives us the possibility to study free shear flows in larger computational boxes at higher Reynolds numbers, significant errors can be introduced by the SGS model. It is thus necessary to use appropriate SGS models for the specific flow case and proper numerical resolution in order to minimize these errors. For this reason, in the framework of the present study, a computation which resembles as closely as possible the DNS (matching initial conditions and computational domain size) was conducted first. The influence of the numerical resolution and SGS model on the statistical quantities of interest and coherent structures were quantified, so that a series of computations with different domain sizes and initial con-

ditions could be carried out with confidence. A similar approach had been followed by Ghosal & Rogers (1997), in conducting LES of turbulent plane wakes. The DNS of Moser, Rogers & Ewing (1998) for the same flow was used as a reference case. From their simulations it is evident that LES can reproduce with accuracy most turbulent statistics of interest as well as the dynamics of coherent structures when compared with DNS for the same conditions (initial and boundary conditions, domain size). Moreover, their computations on larger domains showed that this parameter can affect the evolution of the layer. In addition, they showed that each simulated wake exhibits self-similar behaviour; the wake spreading rates, however, depend on initial conditions.

In the following section the governing equation, simulation method and parameters are described. The numerical algorithm and the subgrid-stress model is validated, and a grid-refinement study is shown. Then the turbulent statistics are presented, followed by a discussion of the topology of the flow. The significance of these results is discussed in some concluding remarks.

2. Problem formulation and simulation parameters

The governing equations for the LES of turbulent mixing layers are the incompressible filtered Navier–Stokes equations, which describe the evolution of the large scales:

$$\frac{\partial \bar{u}_i}{\partial t} + \frac{\partial}{\partial x_j}(\bar{u}_i \bar{u}_j) = -\frac{\partial \bar{P}}{\partial x_i} - \frac{\partial \tau_{ij}}{\partial x_j} + \frac{1}{Re}\frac{\partial^2 \bar{u}_i}{\partial x_j \partial x_j} \tag{2.1}$$

$$\frac{\partial \bar{u}_i}{\partial x_i} = 0, \tag{2.2}$$

where $\bar{P}$ is the pressure, and u_1, u_2 and u_3 (or u, v and w) are the streamwise, spanwise and cross-stream velocity components. All quantities are made dimensionless by the velocity difference between the high- and low-speed sides of the layer, ΔU, and by its momentum thickness at the initial time, θ_0. The momentum thickness is defined as

$$\theta = \int_{-\infty}^{\infty} \left[\frac{1}{4} - \left(\frac{U}{\Delta U}\right)^2\right] \mathrm{d}z. \tag{2.3}$$

Here $U = \langle u \rangle$, and the angle brackets are an average over the plane of homogeneity of the flow (the x, y-plane). The effect of the subgrid scales upon the resolved part of turbulence appears in the subgrid-scale (SGS) stress term $\tau_{ij} = \overline{u_i u_j} - \bar{u}_i \bar{u}_j$, which must be modelled. In the present study the SGS stresses are parameterized using a dynamic eddy-viscosity model of the form

$$\tau_{ij} - \tfrac{1}{3}\delta_{ij}\tau_{kk} = -2\nu_{\mathrm{T}}\bar{S}_{ij} = -2C\Delta^2|\bar{S}|\bar{S}_{ij}, \tag{2.4}$$

in which δ_{ij} is Kronecker's delta and $|\bar{S}| = (2\bar{S}_{ij}\bar{S}_{ij})^{1/2}$ is the magnitude of the large-scale strain-rate tensor,

$$\bar{S}_{ij} = \frac{1}{2}\left(\frac{\partial \bar{u}_i}{\partial x_j} + \frac{\partial \bar{u}_j}{\partial x_i}\right). \tag{2.5}$$

To determine the coefficient C, the Lagrangian averaging procedure proposed by Meneveau, Lund & Cabot (1996) is used. This type of averaging eliminates sharp fluctuations of the coefficient C which tend to destabilize the calculations, while it preserves, to a certain degree, the locality of the model in space. The model has been

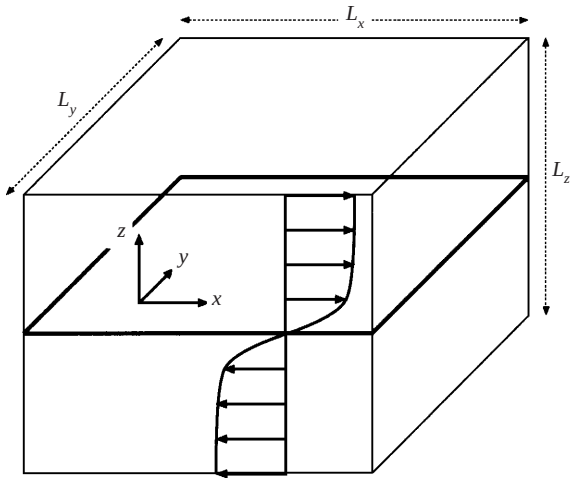

FIGURE 1. Sketch of the computational domain.

found to give accurate predictions in turbulent and transitional flows and is, therefore, well suited to the present numerical calculation that will encompass both flow regimes. A complete analysis of the model can be found in Meneveau *et al.* (1996). Details of the present implementation, together with an evaluation of its accuracy in equilibrium and non-equilibrium flows, are given in Sarghini, Piomelli & Balaras (1999).

The governing equations (2.1) and (2.2) were integrated in time using an Adams–Bashforth fractional-step method. Both advective and diffusive terms were treated explicitly. The equation for the pressure was solved using a direct Poisson solver based on fast Fourier transforms. All spatial derivatives were approximated by second-order central differences on a staggered grid.

A schematic representation of the computational box is shown in figure 1. Periodic boundary conditions were applied in the homogeneous streamwise and spanwise directions. At the open boundaries in the cross-stream direction radiative boundary conditions were used (Gresho & Sani 1987), which allow the flow to enter or exit the computational domain without influencing the solution in the domain near the open boundary.

In order to examine the effect of the initial conditions on the evolution of the layer, two different cases were considered. Following Rogers & Moser (1994), one calculation (Case 1) was started from a field created by taking two different realizations of a turbulent boundary layer LES and bringing them together with their free streams moving in opposite directions. This simulation resembles experiments in which both boundary layers at the end of the splitter plate are turbulent, although the mean vorticity profile across the dividing plane is different from that at the end of splitter plates dividing experimental boundary layers. Another computation (Case 3) was started from the same boundary layer flow fields; however, the three velocity components were individually scrambled in a way that preserved their first- and second-order moments, but removed all phase relationships between them. Such simulations are similar to transitional simulations reported in the literature, albeit with a much higher level of initial perturbations. This choice of initial conditions allowed us to study the effect of boundary layer turbulence on the evolution of the layer, especially at the initial stages of the development. The size of the computational domain was chosen to match approximately that of the Rogers & Moser (1994) DNS.

Case	Domain size ($\times\theta_0$)	Grid size	Initial conditions
1	$L_x = 110, L_y = 28, L_z = 110$	$128 \times 64 \times 128$	BL turbulence
2	$L_x = 220, L_y = 56, L_z = 110$	$256 \times 128 \times 128$	BL turbulence
2A	$L_x = 110, L_y = 56, L_z = 110$	$128 \times 128 \times 128$	BL turbulence
2B	$L_x = 220, L_y = 28, L_z = 110$	$256 \times 64 \times 128$	BL turbulence
3	$L_x = 110, L_y = 28, L_z = 110$	$128 \times 64 \times 128$	Random noise
4	$L_x = 220, L_y = 56, L_z = 110$	$256 \times 128 \times 128$	Random noise

TABLE 1. Computational parameters.

The boundary layer calculations were carried out using the upper part of the domain shown in figure 1 with the same resolution. The Reynolds number, based on the initial boundary-layer momentum thickness and free-stream velocity was $Re_\theta = 330$. The choice of this low Reynolds number, in which the extent of the logarithmic layer is very small, was part of our effort to simulate the conditions in the Rogers & Moser (1994) DNS as closely as possible. In their study the initial boundary-layer Reynolds number was $Re_\theta = 300$.

Both computations were repeated on a larger computational box, twice the size of the first one in the streamwise and spanwise directions (Cases 2 and 4). In order to determine which dimension of the computational box has the largest effect on the layer evolution, two additional computations were conducted. The first (Case 2A), has the same box length in the streamwise direction as Case 1 but is twice as large in the spanwise direction. The situation is reversed (same box length in the spanwise direction, twice as large in the streamwise one) for Case 2B. The grid resolution and simulation parameters are summarized in table 1. The domain size in the cross-stream directions as well as the numerical resolution were kept the same in all six cases, and the initial mixing-layer Reynolds number was $Re_\theta = 900$. As the layer grows, the Reynolds number of course increases; the maximum Reynolds number for the calculations discussed here was $Re_\theta = 3400$.

Note that the parameters that affect the accuracy of the results (grid resolution and subgrid-scale stress model) were the same for all the calculations. In this way, once we have established confidence in the accuracy of the present computations by comparison with the DNS data, we believe that the trends predicted by the LES can be trusted, and meaningful conclusions can be drawn that are unaffected by modelling and resolution errors.

3. Results

3.1. *Simulation validation*

In order to establish the independence of the results from numerical resolution, subgrid-scale model and boundary condition treatment at the free-stream boundaries, a series of computations was carried out prior to the six simulations mentioned in the above paragraphs. Case 1, for which initial conditions and domain size are identical to the reference DNS of Rogers & Moser (1994), was chosen to be the baseline simulation. Computations with half (Case 1A) and double (Case 1B) resolution in the streamwise and spanwise directions, compared to Case 1, were conducted. An additional computation with domain size in the cross-stream direction half that of Case 1, but with the same number of non-uniformly distributed grid points was

Case	Domain size ($\times\theta_0$)	Grid size
1	$L_x = 110, L_y = 28, L_z = 110$	$128 \times 64 \times 128$
1A	$L_x = 110, L_y = 28, L_z = 110$	$64 \times 32 \times 128$
1B	$L_x = 110, L_y = 28, L_z = 110$	$256 \times 128 \times 128$
1C	$L_x = 110, L_y = 28, L_z = 55$	$128 \times 64 \times 128$

TABLE 2. Parameters for the grid refinement study.

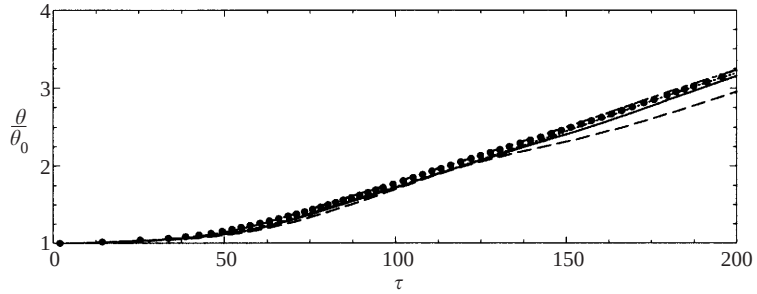

FIGURE 2. Time evolution of θ/θ_0. ●, DNS, Rogers & Moser (1994); ———, Case 1; — — —, Case 1A; ·····, Case 1B; — · —, Case 1C.

also performed (Case 1C). This last case, apart from revealing the influence of grid resolution in the cross-stream plane, can demonstrate the effect of the location of the free-stream boundaries in the evolution of the layer. A summary of all computational parameters for the preliminary study is given in table 2.

In figure 2 the evolution of the normalized mixing-layer momentum thickness θ/θ_0 (where θ_0 is the initial momentum thickness) as a function of non-dimensional time $\tau = t\Delta U/\theta_0$ is shown for all cases. During the evolution of the coarse resolution case (Case 1A) deviation from the expected linear behaviour can be observed. The slope of the curve changes several times. This could be due to the fact that this resolution is inadequate to resolve all essential structures present in the flow. In addition the reduced spatial sample in this case can contribute to the difference. For these reasons, and because a clear self-similar period could not be identified, this case was discarded.

For all other cases, after an initial adjustment period, θ/θ_0 grows linearly with time. The agreement with the reference DNS data is very good and the differences between the baseline computation (Case 1) and the refined computations (Cases 1B and 1C) are negligible. In the linear region the non-dimensional growth rate based on the momentum thickness defined as

$$r_\theta = \frac{1}{\Delta U}\frac{\mathrm{d}\theta}{\mathrm{d}t} = \frac{\mathrm{d}(\theta/\theta_0)}{\mathrm{d}\tau}, \tag{3.1}$$

is $r_\theta = 0.014$ for all three cases. This is identical with the value reported in Rogers & Moser (1994) for their unforced simulation.

For all three cases (Cases 1, 1B and 1C) the extent of the self-similar period was the same (see § 3.2 for details) and approximately extended over the interval $120 < \tau < 200$. The reference DNS self-similar period is different and extends over a $105 < \tau < 150$ interval. Several reasons can explain this difference. First, the initial condition in the DNS was taken from a calculation (Spalart 1988) in which a multiple-scale procedure was applied to approximate the streamwise growth of the boundary

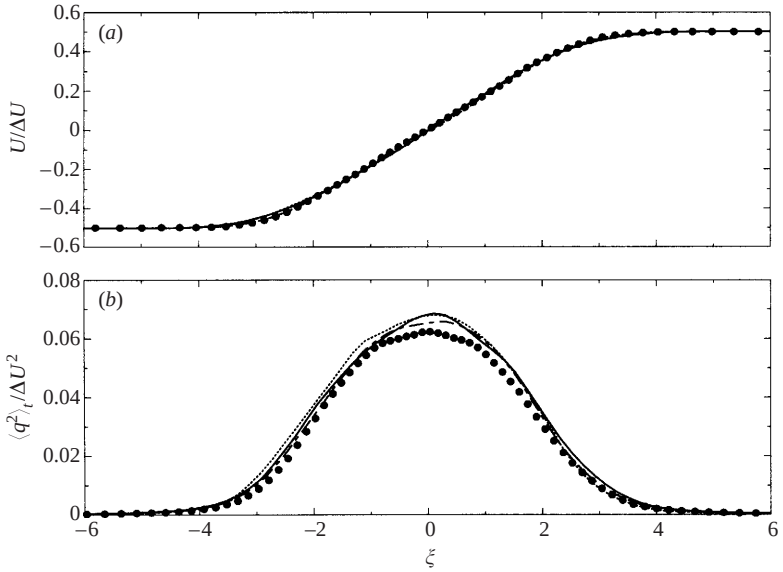

FIGURE 3. (*a*) Space–time-averaged streamwise velocity in similarity coordinates; (*b*) space–time-averaged resolved turbulent kinetic energy in similarity coordinates. ●, DNS, Rogers & Moser (1994); ———, Case 1; ·····, Case 1B; —·—, Case 1C.

layers; in the present simulations actual spatially developing LES were conducted to create the boundary-layer fields. Secondly (and perhaps most importantly) some degree of subjectivity is necessarily introduced when judging the extent of the self-similar region, for example in the identification of the region in which the total dissipation (shown later) is flat.

The time-averaged mean velocity U over this period and the corresponding resolved turbulent kinetic energy $\langle q^2\rangle_t = \langle \bar{u}_i\bar{u}_i\rangle_t$ plotted in similarity coordinates, are shown in figure 3. In the following, while the angle brackets continue to denote the average of a quantity over the (x, y)-plane, ensembles obtained by averaging over planes and time are denoted by $\langle\ \rangle_t$. The predicted mean velocity profiles (figure 3*a*) are nearly identical for all cases, and in very good agreement with the DNS data. The turbulent kinetic energy $\langle q^2\rangle_t$ (figure 3*b*) is slightly over-predicted, by approximately 8%, compared to the DNS data. The difference in the initial conditions could be also responsible for this discrepancy. The fact, however, that this behaviour, was also observed in well-resolved finite-difference simulations of wall bounded flows, indicates that it could also be due to modelling errors. Nevertheless, this is a satisfactory result, taking into account that the present simulations use only a fraction of the grid points used in the DNS. The computations with different grid resolution, moreover, agree well with each other. The maximum differences between them close to the centreline are about 2%, which is probably within the uncertainty introduced by the size of the statistical sample in these temporal simulations.

In summary, the resolution chosen for the baseline simulation (Case 1) is sufficient to resolve adequately all large energy-carrying structures. Increasing the number of grid points in the streamwise, spanwise and cross-stream directions by a factor of 2 appears to have minimal influence on the results. Furthermore, statistical quantities agree well with the reference DNS data reported by Rogers & Moser (1994) (see also § 3.2 for a detailed comparison). This indicates that LES coupled with the Lagrangian

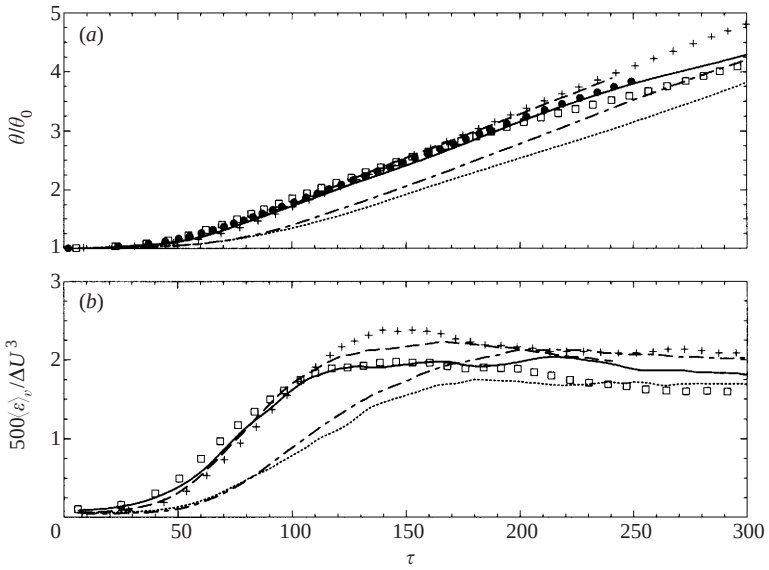

FIGURE 4. Time evolution of (*a*) θ/θ_0, (*b*) $500\langle\varepsilon\rangle_v/\Delta U^3$. ●, DNS, Rogers & Moser (1994); ———, Case 1 (small box, boundary layer turbulence); — — —, Case 2 (large box, boundary layer turbulence); +, Case 2A (box doubled in the spanwise direction only); □, Case 2B (box doubled in the streamwise direction only); ·····, Case 3 (small box, random noise); —·—, Case 4 (large box, random noise).

dynamic eddy-viscosity model represents very accurately the energy exchange between large and small scales in free shear layers. A similar conclusion was drawn by Vreman *et al.* (1997). They examined the accuracy of several SGS models for the case of a temporally evolving mixing layer, and found that dynamic eddy-viscosity models predict all velocity statistics very accurately. In addition, the correct amount of SGS dissipation was provided by the model, as demonstrated by the comparison of filtered DNS energy spectra and turbulent kinetic energy dissipation with the LES data. Having established this, in the following sections the effects of initial conditions and domain size on the growth of the layer towards self-similarity, statistical quantities and coherent structures will be examined in detail.

3.2. *Self-similarity*

After an initial adjustment period, turbulent mixing layers are known to evolve self-similarly. As described above, the self-similar state is characterized by the linear growth of the layer thickness and turbulent statistics that, when scaled by the appropriate variables, are independent of the downstream position (or the position in time for temporally evolving computations). A detailed evaluation of the degree to which these self-similarity criteria are met in all the four cases simulated in this study has been performed, and will be discussed next.

In figure 4(*a*) the evolution of the normalized mixing-layer momentum thickness θ/θ_0 as a function of non-dimensional time τ is shown. After an initial transient, θ/θ_0 grows linearly with time in all cases. For Case 1 the layer starts to evolve linearly after $\tau \simeq 70$, with a non-dimensional growth-rate $r_\theta = 0.014$. When the domain is doubled in the streamwise and spanwise directions (Case 2) the initial adjustment stage is approximately the same as in Case 1 until $\tau \simeq 90$; after this time, however, Case 2 grows at a faster rate, $r_\theta = 0.015$. This is an indication that the domain size can affect

the layer growth, perhaps by restricting the large-structure evolution. In figure 4(*a*) the evolution of the layer is also shown for Cases 2A and 2B where the computational domain is doubled only in the spanwise or streamwise directions respectively. The behaviour of θ/θ_0 for Case 2A is very similar to that in Case 2, indicating that the spanwise extent of the box is responsible for most of the difference. Case 2B is very close to Case 1 (small domain) until $\tau \simeq 180$. After this point a drastic change in the slope can be observed, probably a product of interactions between quasi-two-dimensional structures. This trend can also be observed in the dissipation that will be discussed next.

The same trend, as far as the domain size is concerned, can be seen for Cases 3 and 4, which start from random noise. The growth rates are $r_\theta = 0.012$ and 0.0135 for Cases 3 and 4 respectively. In addition, for Cases 3 and 4 self-preservation is established at a later time. This is more evident in figure 4(*b*), in which the integrated rate of dissipation of turbulent kinetic energy,

$$\langle \varepsilon \rangle_v = \frac{1}{L_x L_y} \int_0^{L_z} \int_0^{L_y} \int_0^{L_x} \varepsilon \, \mathrm{d}x \, \mathrm{d}y \, \mathrm{d}z, \quad \varepsilon = 2\nu \bar{S}_{ij} \bar{S}_{ij} - \tau_{ij} \bar{S}_{ij}, \tag{3.2}$$

is shown. We recall that in equation (3.2) $\bar{S}_{ij}$ is the resolved strain rate and τ_{ij} is the subgrid-scale stress. This quantity, which is scaled by ΔU^3 becomes approximately constant during the self-similar period (see Rogers & Moser 1994). The computations started from random noise became self-similar at approximately $\tau \simeq 200$, much later than the beginning of self-similarity at $\tau \simeq 120$ for the cases started from boundary layer turbulence; $\langle \varepsilon \rangle_v$ also reaches a brief plateau at $\tau \simeq 120$ in the Rogers & Moser (1994) DNS. This result is consistent with the trends reported in experimental studies of single- and two-stream mixing layers. For example, in the Bell & Mehta (1990) experiment, in which the range of Reynolds numbers is comparable to the one in the present computations, most turbulent quantities plotted in similarity coordinates begin collapsing further downstream when the boundary layers at the edge of the splitter plate are laminar, compared with cases in which the boundary layers are turbulent.

In addition to the integrated quantities, the resolved velocity fluctuation second-moment statistics have also been examined for self-similarity. In figure 5, iso-lines of mean velocity and streamwise velocity variance $\langle u'u' \rangle$, are shown for the large-box, random-noise case (Case 4). The horizontal axis is the non-dimensional time τ, and the vertical one is the normalized similarity coordinate $\xi(\tau) = y/\theta(\tau)$. After an initial adjustment period, the iso-lines become approximately parallel, indicating self-similar evolution. Towards the end of the calculation, however, self-similarity breaks down as illustrated by the fact that the iso-lines are no longer parallel. The length of the self-similar period appears to be insensitive to the box size. Based on evolution of $\langle \varepsilon \rangle_v$ one can conclude that the self-similar period is extended for both cases in the large box. A detailed examination of the individual velocity statistics, however, shows a loss of self-similar scaling for some of the statistics (the streamwise velocity fluctuations for example). For this reason identical self-similar periods were considered when comparing corresponding statistics during self-similar evolution. In the DNS study of Rogers & Moser (1994) it was conjectured that the breakdown of self-similarity is due to two-dimensionality of the spanwise rollers, resulting, in the late stages of development, from the limited extent of the computational domain in the spanwise direction. From the considerations above it is clear that other factors are involved that require further investigation.

Case	Beginning	End
1 (small box, BL turbulence)	125	200
2 (large box, BL turbulence)	125	200
3 (small box, random noise)	200	280
4 (large box, random noise)	200	280

TABLE 3. Averaging times for the various calculations.

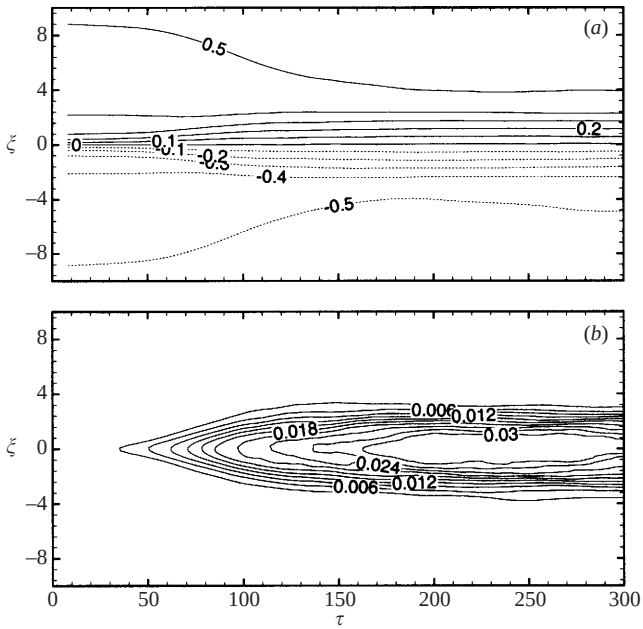

FIGURE 5. Time evolution of (*a*) $U/\Delta U$; (*b*) $\langle u'u' \rangle / \Delta U^2$. Case 4 (large box, random noise).

To increase the statistical sample, turbulence statistics can be averaged over the self-similar period of the evolution. Since the beginning and end of the self-similar period are different for each statistical quantity, in the present work the averages were taken over the period in which all quantities of interest appeared to have reached self-similarity, as indicated by their iso-lines and by sample profiles. In table 3 the initial and final times of the self-similar period for the four cases examined are reported.

3.3. *Turbulence statistics*

The time- and space-averaged mean-velocity profiles are shown in figure 6. The velocity profiles for all four of the present LES cases are nearly identical and agree well with the DNS data. In figure 7 the velocity variances are shown. Case 1 is in generally good agreement with the DNS data, further confirming the accuracy of LES that use the Lagrangian dynamic eddy-viscosity model, at least at the resolution used here. The peak of the LES distribution of $\langle u'u' \rangle_t$ is greater than that of the DNS, and both have somewhat anomalous shapes near the peaks. The LES distribution of $\langle w'w' \rangle_t$ is slightly higher than that of DNS all across the layer.

Initial conditions and domain size, however, affect the results significantly. The large-domain calculations have higher fluctuation levels than the small box ones.

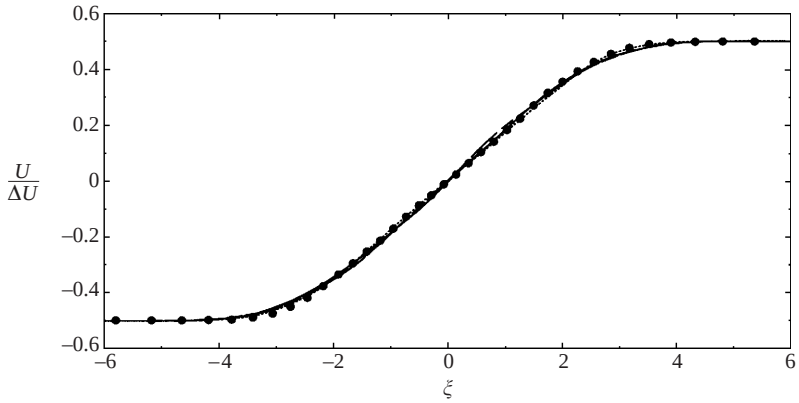

FIGURE 6. Space–time-averaged streamwise velocity in similarity coordinates. ●, DNS, Rogers & Moser (1994); ———, Case 1 (small box, BL turbulence); — — —, Case 2 (large box, BL turbulence); ·····, Case 3 (small box, random noise); —·—, Case 4 (large box, random noise).

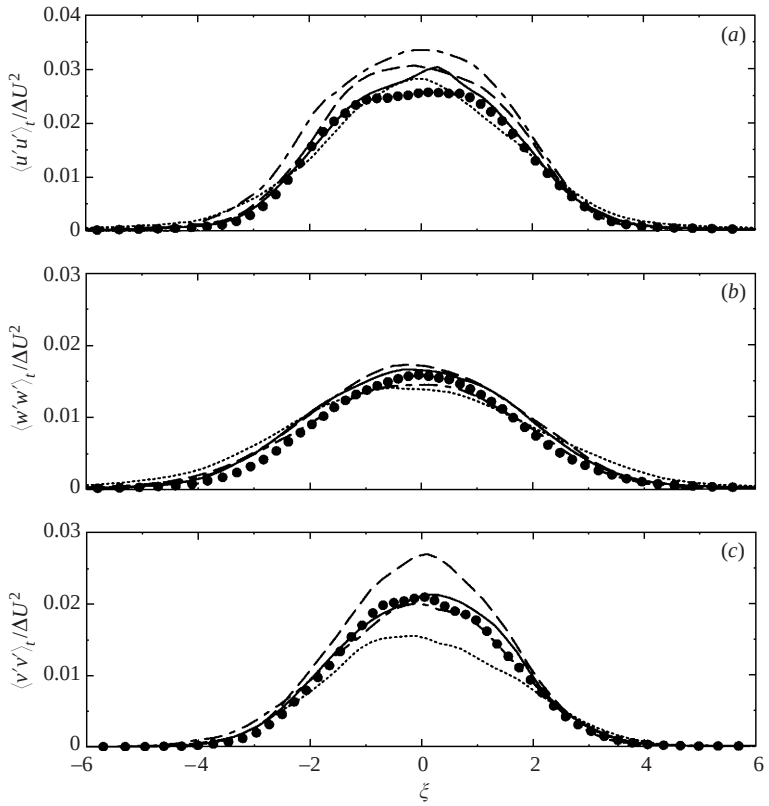

FIGURE 7. Space–time-averaged velocity variances in similarity coordinates. (*a*) Streamwise; (*b*) cross-stream; (*c*) spanwise. ●, DNS, Rogers & Moser (1994); ———, Case 1 (small box, BL turbulence); — — —, Case 2 (large box, BL turbulence); ·····, Case 3 (small box, random noise); —·—, Case 4 (large box, random noise).

In particular, the streamwise velocity variances for Cases 3 and 4, which are both initialized with random noise and carried out on small and large computational domains respectively, differ by approximately 21% at the centreline. For the spanwise variances the additional effect of the differences between the turbulent and random noise initial conditions can be clearly observed. The Case 2 peak is 38% greater than that of Case 4. The combined effects give an approximately 83% increase in the Case 2 peak compared to the Case 3 peak for $\langle v'v' \rangle_t$. While some level of discrepancy between the various data sets may be attributed to insufficient sample, the differences mentioned here are far above the uncertainties of the present calculation. The significant differences in the spanwise variance levels are a particularly important indicator of more highly three-dimensional flow patterns in the cases initialized with boundary-layer turbulence and in the large-domain calculations. This issue is investigated further in § 3.4.

The statistical data presented here show that, although self-similar states are reached independently of the initial conditions and parameters of the simulation, *they are not the same self-similar states*. The initial conditions and the computational domain size affect the turbulent statistics significantly. The substantial differences between the spanwise velocity peak variances indicate that the self-similar states differ in their degree of three-dimensionality. The large structures should be affected, a conclusion that is supported to some extent by the experimental finding of Bell & Mehta (1990) regarding the peak of secondary shear stress. To investigate this conjecture further, the instantaneous velocity fields will be examined below to determine the structure of the coherent vortices and how their evolution and dynamics are affected by the initial conditions and computational domain size.

3.4. *Coherent structures*

Here we will examine the instantaneous velocity fields to illustrate how the statistical differences observed before are reflected in a different flow structure in each of the cases computed. We will first compare the two most extreme cases and show the significantly different shapes of the coherent eddies during the self-similar period. Then, we will examine the development of the layers into self-similarity, beginning from their early stages. Thus, we will be able to highlight the effect of initial conditions and domain size.

Several methods can be used in numerical simulations to visualize the coherent eddies in a turbulent flow. Robinson (1991) compared various techniques, and found that the pressure is effective in identifying the regions of strong rotation in vortex cores. Hunt, Wray & Moin (1988) proposed the use of the second invariant of the velocity-gradient tensor,

$$Q = -\frac{1}{2}\frac{\partial u_i}{\partial x_j}\frac{\partial u_j}{\partial x_i} = -\tfrac{1}{2}(S_{ij}S_{ij} - \Omega_{ij}\Omega_{ij}), \tag{3.3}$$

where S_{ij} and Ω_{ij} are, respectively, the strain-rate and rotation tensors (that is, the symmetric and anti-symmetric parts of the velocity-gradient tensor). In the present study both tensors are evaluated using resolved quantities. In regions where $Q > 0$ the vorticity is significant and is due to rotation rather than to shear. We found that the low-pressure regions highlight the rollers very effectively, but only the strongest rib vortices are visualized well by this technique. Conversely, the $Q > 0$ criterion is more effective at highlighting the rib vortices. Both criteria will be used in the following.

In figure 8, iso-surfaces of P and Q are shown for Cases 2 and 3 during the self-similar period at $\theta/\theta_0 = 2.6$. In this and following figures, the coordinates have

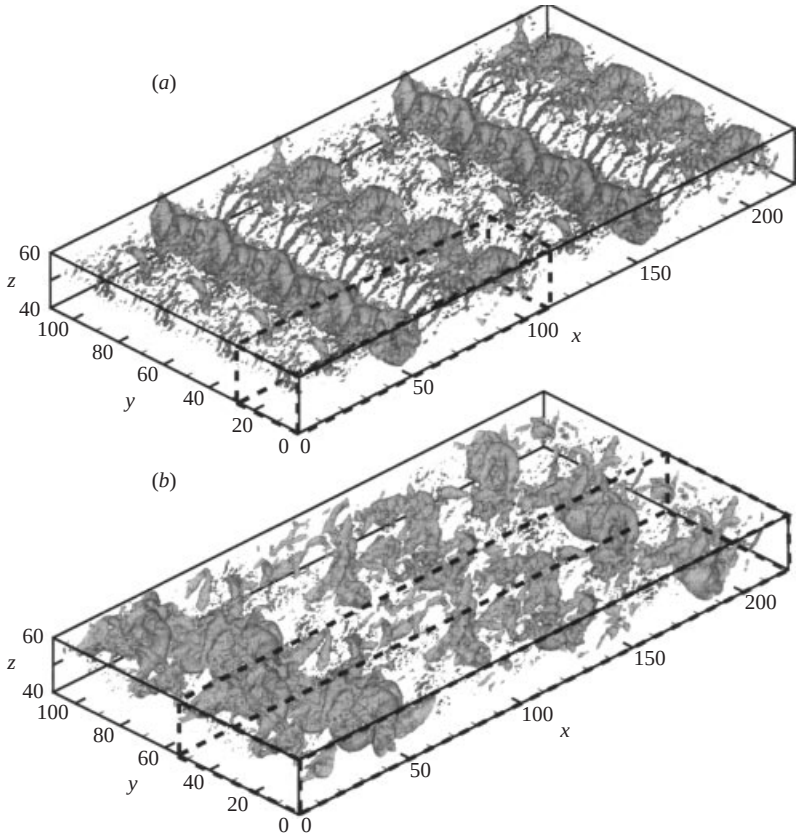

FIGURE 8. Iso-surfaces of P and Q during the self-similar period ($\theta/\theta_0 = 2.6$). (*a*) Case 3 (small box, random noise); (*b*) Case 2 (large box, BL turbulence). The large domain is repeated twice in the spanwise direction, and the small one three times in the spanwise and twice in the streamwise directions, for clarity. The iso-surface levels are $P = -0.04\Delta U^2$ (lighter grey) and $Q = 0.08\Delta U^2/\theta_0^2$ (darker grey). In this and following figures, the coordinates have been normalized with the initial momentum thickness.

been normalized with the initial momentum thickness of the layer and the small-box calculations have been extended periodically in the x- and y-directions in order to facilitate the comparison with the large-box ones. The size of the actual computational box for both cases is marked with the dashed line in figure 8. A significant difference is apparent between the two realizations. The small-domain, random-noise calculation shows a fairly well-organized structure, even at this late stage of the evolution. A regular array of quasi-two-dimensional rollers can be observed, with strong rib vortices in the braid region. The large-domain, boundary-layer turbulence simulation, on the other hand, displays a much more chaotic structure. The rollers are significantly twisted, and the braid regions are essentially devoid of rib vortices. Only very weak remnants of the coherent vorticity present in the ribs can be observed. The topological features of the flow support the conjecture that the more highly three-dimensional structure of the large-scale eddies in the latter case is responsible for the difference in the similarity states, characterized most prominently by the different dissipation levels and significantly higher spanwise-velocity variances discussed earlier.

The evolution of the layer in Case 3 (small box, random noise) is shown in figure 9. Initially, the most unstable mode (given by the linear stability analysis with the mean

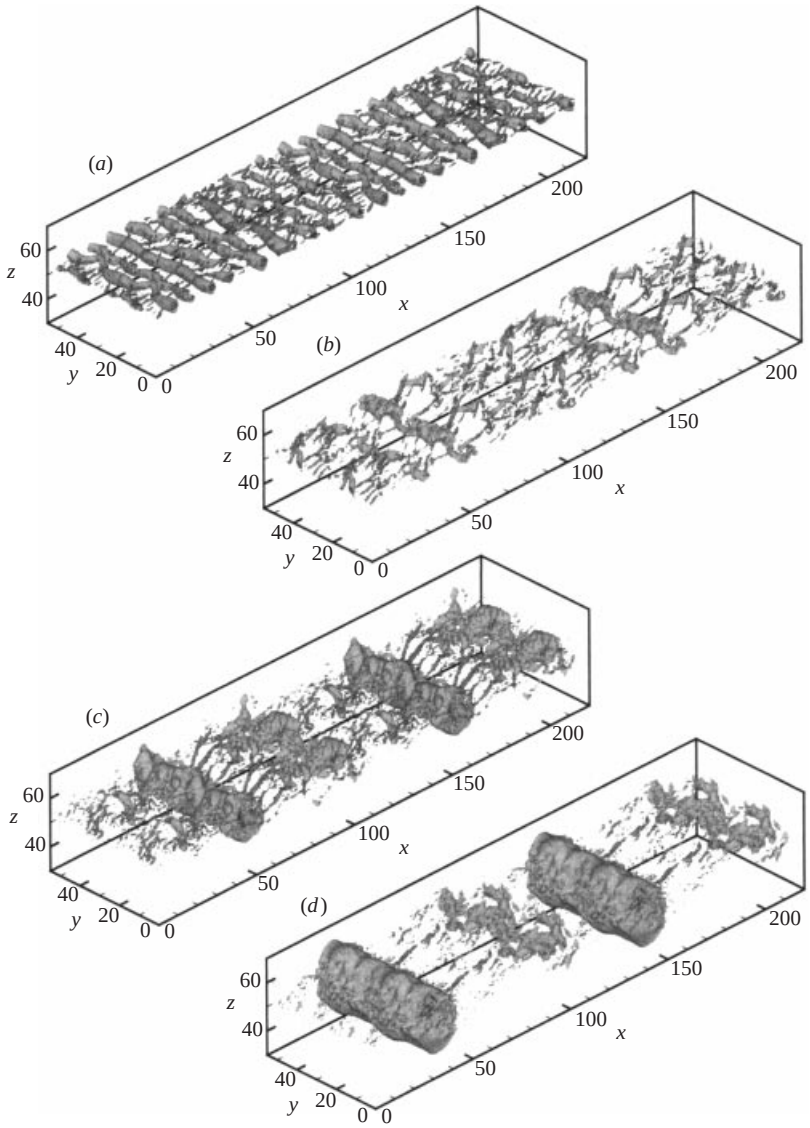

FIGURE 9. Iso-surfaces of P and Q during the evolution of the mixing layer. Case 3 (small box, random noise). (*a*) $\theta/\theta_0 = 1.1$; (*b*) $\theta/\theta_0 = 1.6$; (*c*) $\theta/\theta_0 = 2.6$; (*d*) $\theta/\theta_0 = 3.4$. The domain is repeated twice in the spanwise and streamwise directions. The iso-surfaces of P are in lighter grey, those of Q in the darker grey. Iso-surface levels are: (*a*) $P = -0.02\Delta U^2$, $Q = 0.01\Delta U^2/\theta_0^2$; (*b*) $P = -0.06\Delta U^2$, $Q = 0.07\Delta U^2/\theta_0^2$; (*c*) $P = -0.04\Delta U^2$, $Q = 0.06\Delta U^2/\theta_0^2$; (*d*) $P = -0.04\Delta U^2$, $Q = 0.06\Delta U^2/\theta_0^2$.

velocity profile as the base flow) begins to grow. The wavelength of this mode is approximately $9\theta_0$, which corresponds to an array of 25 spanwise rollers for the domain shown in the figure. Pairings then begin to take place, and by the time corresponding to $\theta/\theta_0 = 1.1$, a spacing between rollers of approximately $10\theta_0$ can be observed.

An enlargement of the coherent structures for Case 3 and $\theta/\theta_0 = 1.1$ is shown in figure 10. Several rollers undergoing helical pairings can be seen (denoted by A in figure 10, for instance). Some very regular, nearly two-dimensional rollers are also

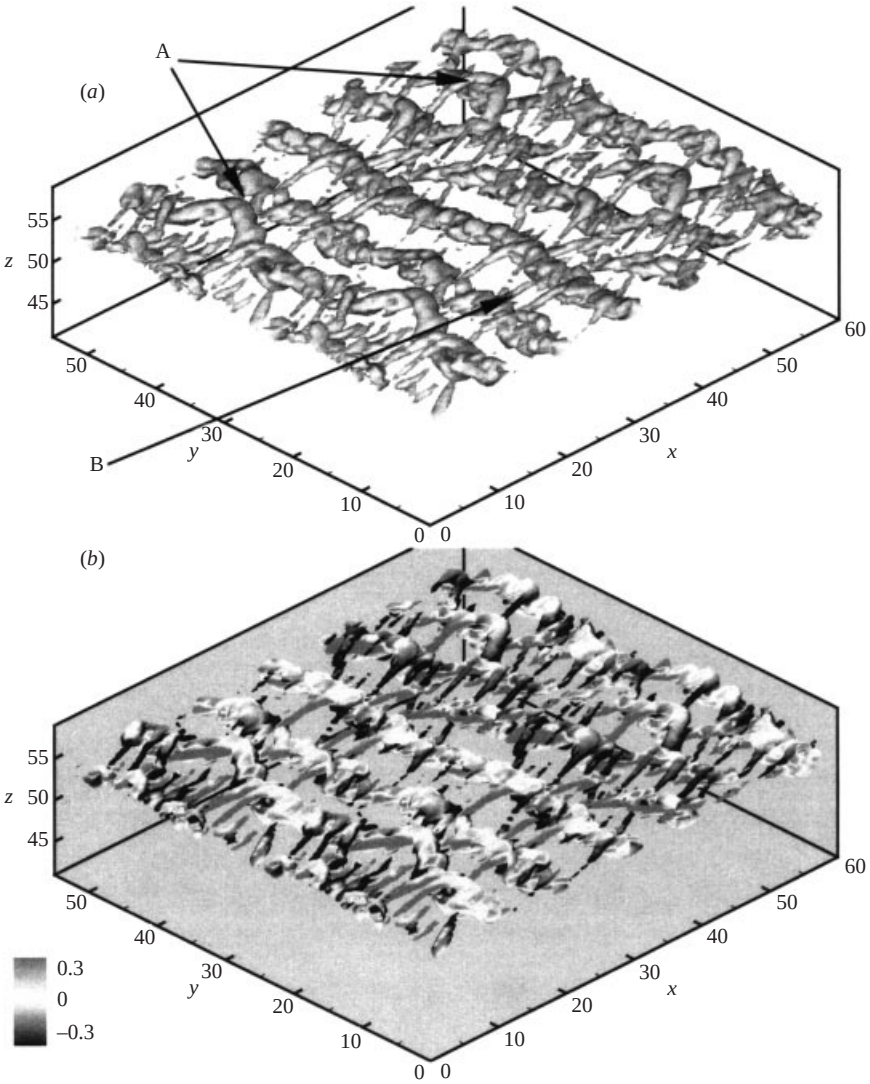

FIGURE 10. Coherent eddies during the early times of the evolution ($\theta/\theta_0 = 1.1$). Case 3 (small box, random noise). (*a*) Iso-surfaces of $Q = 0.01\Delta U^2/\theta_0^2$; (*b*) iso-surfaces of Q coloured according to the streamwise vorticity.

present. The rib vortices (one is indicated by B) span the braid region, wrapping over the downstream roller and under the upstream one. Their streamwise vorticity (figure 10*b*) can be of either sign, and no alternating pattern of positive and negative rib vortices can be detected, as also observed by Comte *et al.* (1998). In the rollers, very little streamwise vorticity is observed, as expected, except where they form kinks and the spanwise component is turned into streamwise vorticity.

As time progresses, more pairings take place and the number of rollers present in the domain decreases, as seen in figure 9. At $\theta/\theta_0 = 1.6$ the spacing between rollers is approximately $18.3\theta_0$. Fairly strong rib vortices can be observed in the braid regions, and these vortices are still present during the self-similar stages ($\theta/\theta_0 = 2.6$) at which time a spacing between rollers of approximately $55\theta_0$ is observed.

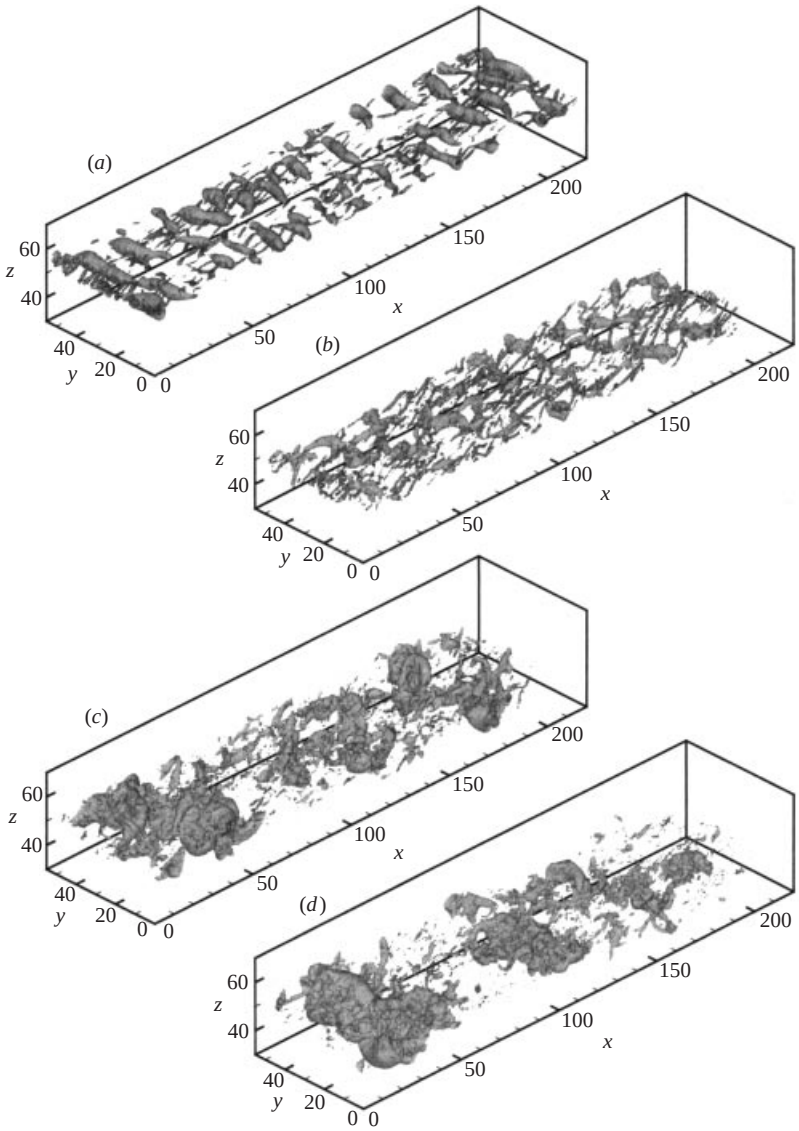

FIGURE 11. Iso-surfaces of P and Q during the evolution of the mixing layer. Case 2 (large box, boundary layer turbulence). (*a*) $\theta/\theta_0 = 1.1$; (*b*) $\theta/\theta_0 = 1.6$; (*c*) $\theta/\theta_0 = 2.6$; (*d*) $\theta/\theta_0 = 3.4$. The iso-surfaces of P are in lighter grey, those of Q in the darker grey. Iso-surface levels are: (*a*) $P = -0.02\Delta U^2$, $Q = 0.01\Delta U^2/\theta_0^2$; (*b*) $P = -0.06\Delta U^2$, $Q = 0.07\Delta U^2/\theta_0^2$; (*c*) $P = -0.04\Delta U^2$, $Q = 0.08\Delta U^2/\theta_0^2$; (*d*) $P = -0.04\Delta U^2$, $Q = 0.08\Delta U^2/\theta_0^2$.

Examination of the sequence of images leading to figure 9(*c*) reveals that the structure of the flow at $\theta/\theta_0 = 2.6$ results from the evolution of an array of six vortices in which two pairs (the second and third and the fifth and six) approach each other and undergo pairing. This leads to an increased distance between the pairing vortices and the one immediately following them downstream. The increased distance between the rollers causes the rib vortices to be stretched, decreasing their diameter and making the viscous diffusion effects more significant. At the late stages of development, $\theta/\theta_0 = 3.4$, two very large two-dimensional rollers are established, and

no coherent rib vortices can be discerned. At this time, the computational domain appears to affect the results significantly. Breakdown of the self-similarity can be attributed, for this case, to the rollers being forced by end effects to become more two-dimensional, as conjectured by Hussain (1980) and also observed by Rogers & Moser (1994).

A significantly different evolution can be observed for Case 2 (large box, boundary-layer turbulence), in figure 11. First, during the initial stages, the flow is more three-dimensional, weaker rollers are present, and their wavelength is greater than in Case 3. It can be conjectured that this difference is due to the initial conditions. When random noise is used, the energy spectrum at the initial stages is nearly flat. This allows the inviscid instability to play a dominant role, and, as shown, spanwise rollers are observed whose wavelength is that of the Kelvin–Helmholtz instability and rib vortices form quickly. When boundary-layer turbulence is used, on the other hand, the energy content of longer-wavelength structures is relatively more significant (the energy spectrum at $\tau = 0$ decays by approximately 4 orders of magnitude with wavenumber). In this case, the inviscidly most unstable mode of the mean velocity profile does not grow as rapidly, perhaps due to a saturation phenomenon or to the early presence of coherent three-dimensional eddies, and initially the rib vortices are not as well defined.

As time progresses, however, coherent rollers emerge, and a roller–braid pattern can be observed in figure 11(*b*). This pattern is quite similar to the one seen in figure 9(*b*), albeit less coherent in the spanwise direction. This decreased spanwise coherence persists through the self-similar period (figure 11*c*) and continues after the breakdown of similarity (figure 11*d*). A much more three-dimensional structure persists compared with the random-noise calculation shown before.

In figure 12 the turbulent structures are shown for all cases during the initial stages of the evolution ($\theta/\theta_0 = 1.1$). Only minor differences are due to the box size. For different box sizes the two cases initialized with boundary-layer turbulence look very similar (figures 12*a*, *c*), as do those initialized with random noise (figures 12*b*, *d*). By contrast, the initial conditions have a more profound effect at this early stage. When boundary-layer turbulence is used the growth of the most unstable mode is hindered by the presence of longer-wavelength eddies, and the flow develops three-dimensionalities more rapidly than in the cases initialized with random noise.

During the self-similar period, on the other hand, the box size appears to have a substantial effect on the evolution of the large structures, more significant than that of the initial conditions. In figure 13 turbulent structures are shown for all cases at times which correspond to $\theta/\theta_0 = 2.6$. One can observe a more orderly structure for the cases started from random noise (compare figures 13*a* and 13*b*, for instance), but a more significant difference exists between the small-box and the large-box calculations. In fact, even Case 4, which was initialized with random noise, has a significantly more three-dimensional structure than either Cases 1 or 3. Consistent with the findings of Rogers & Moser (1994) the present calculations show that if the diameter of the rollers becomes comparable with their spanwise dimensions, the three-dimensionality of the mixing layer is inhibited, and a more regular topology results.

4. Conclusions

Large-eddy simulations of temporally evolving, turbulent mixing layers have been performed. The simulation parameters were designed with the intent of studying both qualitatively and quantitatively the effect of initial conditions and domain size on

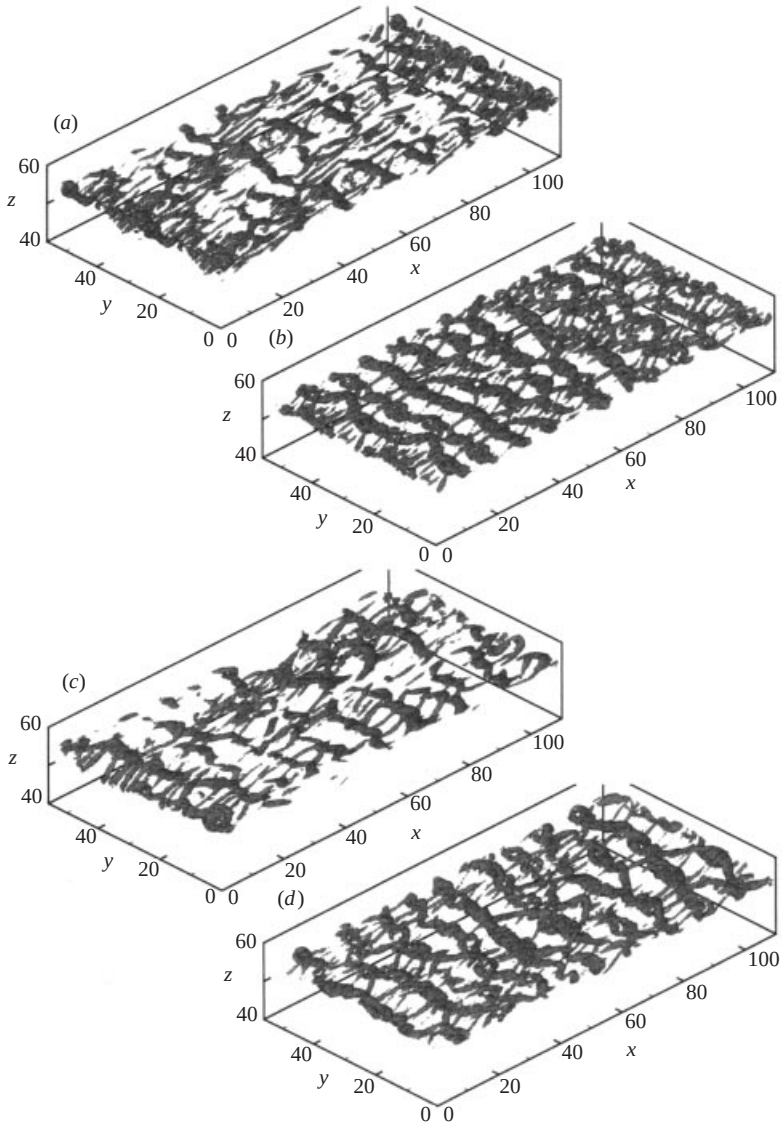

FIGURE 12. Iso-surfaces of $Q = 0.01\Delta U^2/\theta_0^2$ during the early times of the evolution ($\theta/\theta_0 = 1.1$). (*a*) Case 1 (small box, BL turbulence); (*b*) Case 3 (small box, random noise); (*c*) Case 2 (large box, BL turbulence); (*d*) Case 4 (large box, random noise).

the evolution of the layer, and in particular on the self-similar states that resulted. A baseline calculation was carried out that matched the parameters of the DNS of Rogers & Moser (1994). The initial conditions were obtained from two realizations of turbulent boundary layers that were juxtaposed with mean velocities going in opposite directions; the layer was then allowed to grow in time. The mixing-layer momentum thickness and the integral across the layer of the dissipation rate compare very well with the DNS data. Likewise, the mean velocity distributions and the velocity fluctuation variances compare well, except for small differences in the peak values of the variances. Another calculation was carried out with the same initial conditions, but in a domain with extent in the spanwise and streamwise directions doubled in

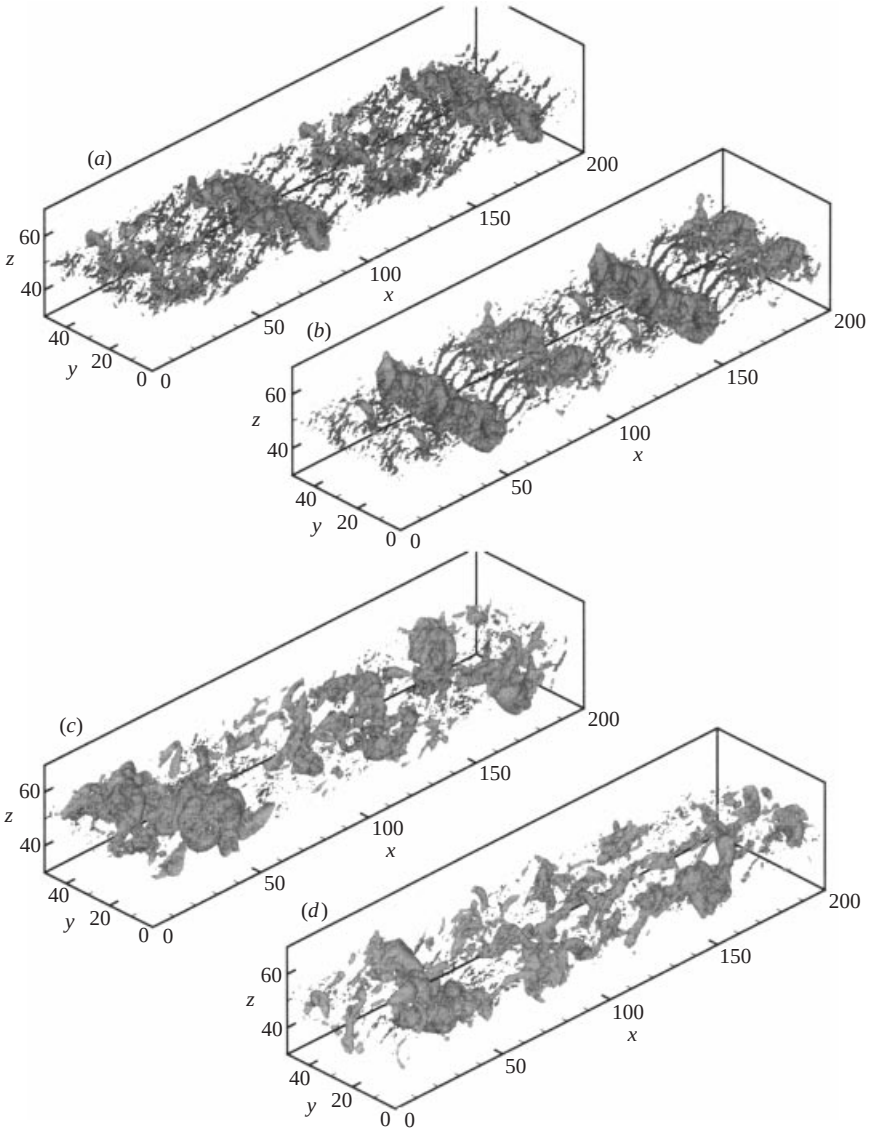

FIGURE 13. Iso-surfaces of Q during the early times of the evolution ($\theta/\theta_0 = 2.6$). (*a*) Case 1 (small box, BL turbulence); (*b*) Case 3 (small box, random noise); (*c*) Case 2 (large box, BL turbulence); (*d*) Case 4 (long box, random noise).

order to study the effects of the box size. To investigate the effects of the initial conditions on the layer development, two additional calculations were carried out in which the initial field was random, but with the same mean velocity and velocity variances as in the turbulent boundary-layer initial condition case. Both small-box and large-box calculations were performed.

Great care was used to determine whether self-similar states were achieved. In addition to the integral quantities, first- and second-order velocity component moments were also examined. In all six cases simulated the mixing layers evolved into self-similar states; the non-dimensional times they began and ended depended strongly, however, on the initial conditions. Furthermore, the self-similar states reached were

not the same. The turbulent statistics and the structure of the flow were significantly affected both by the initial conditions and by the computational domain size. The availability of three-dimensional unsteady fields allowed us to investigate these effects more in detail than done in previous studies. In particular it was found that the initial conditions and the size of the flow domain influence the shape of the coherent eddies of the flow and its statistics. The differences persist throughout the layer development, well into the self-similar period.

In general, the use of a smaller domain forces the spanwise rollers to be two-dimensional during the late stages of the evolution. This results in a regular, well-ordered flow structure. The initial conditions, not surprisingly, have an even stronger effect, particularly on the initial stages of the evolution. The use of random noise lets the Kelvin–Helmholtz instability emerge, leading to the early formation of a regular array of spanwise rollers. When boundary-layer turbulence is used to initiate the layer, on the other hand, the growth of the inviscid instability is inhibited by the presence of lower-wavenumber modes with significant energy content. The result is a delayed formation of the regular array and an initial structure that is more three-dimensional and with longer wavelength. Although more notable during the early stages of the layer development, the differences due to the initial conditions persist throughout the self-similar period.

The differences in the structure of the turbulent flow field are reflected in the statistics of the turbulent quantities, most notably the spanwise velocity fluctuation variance $v'v'$, which is a measure of the three-dimensionality of the flow. The use of the small computational domain resulted in a 20% decrease in this term; the use of random noise to initialize the flow field reduces this term by approximately the same amount.

One conclusion of this work is a confirmation of the experimental and theoretical findings that, although mixing layers evolve into self-similar states, these states are not unique, and may be affected by many factors. Several researchers have conjectured the existence of multiple self-similar states. The possible effect of the domain size, for instance, has been raised by Hussain (1980) for experiments and by Rogers & Moser (1994) based on their DNS results. Numerous experiments have observed differences due to the state of the boundary layer at the splitter plate. However, the fact that experimental and DNS data, or data obtained from different experimental configurations have been routinely compared implies a common belief that the self-similar state is more or less unique. The present calculations are a conclusive demonstration that this is not the case.

Of course, the above conclusions strictly hold only for temporally developing flows. Spatially developing flows have differences in the sign of the mean vorticity and in the inclination of the turbulent eddies near the trailing edge of the plate. In experiments, the presence of the trailing edge may also affect the flow field. The present calculations, however, at the very least suggest that caution should be used when making comparisons between computational and physical experiments.

Financial support for this work was provided by the National Science Foundation under Grant CTS-961862.

REFERENCES

Batt, R. G. 1975 Some measurements on the effect of tripping the two-dimensional shear layer. *AIAA J.* **13**, 245–247.

Bell, J. H. & Mehta, R. D. 1990 Development of a two-stream mixing layer from tripped and untripped boundary layers. *AIAA J.* **28**, 2034–2042.

Bradshaw, P. 1966 The effect of initial conditions on the development of a free shear layer. *J. Fluid Mech.* **26**, 225–236.

Brown, G. L. & Roshko, A. 1974 On density effects and large structure in turbulent mixing layers. *J. Fluid Mech.* **64**, 775–816.

Browand, F. K. & Latigo, B. O. 1979 Growth of the two-dimensional mixing layer from a turbulent and non-turbulent boundary layer. *Phys. Fluids* **22**, 1011–1019.

Cantwell, B. J. 1981 Organized motion in turbulent flow. *Ann. Rev. Fluid Mech.* **13**, 437–515.

Comte, P., Silvestrini, J. H. & Bégou, P. 1998 Streamwise vortices in large-eddy simulations of mixing layers. *Eur. J. Mech.* B/*Fluids* **17**, 615–637.

Dimotakis, P. E. & Brown, G. L. 1976 The mixing layer at high Reynolds number: large-structure dynamics and entrainment. *J. Fluid Mech.* **78**, 535–560.

Dimotakis, P. E. 1991 Turbulent free shear layer and combustion. In *High-Speed-Flight Propulsion Systems*. Progress in Astronautics and Aeronautics, vol. 137, pp. 265–340. AIAA.

Dziomba, B. & Fiedler, H. E. 1985 Effect of initial conditions on two-dimensional free shear layers. *J. Fluid Mech.* **152**, 419–442.

George, W. K. 1989 The self-preservation of turbulent flows and its relation to initial conditions and coherent structures. In *Advances in Turbulence*, Hemisphere, NY, 39–73.

Ghosal, S. & Rogers, M. M. 1997 A numerical study of self-silarity in a turbulent plane wake using large-eddy simulation. *Phys. Fluids* **9**, 1729–1739.

Görtler, H. 1942 Berechnung von aufgaben der frein turbuleuz auf grund eines neuen nahrungsansatzes. *Z. Angew. Math. Mech.* **22**, 244–254.

Gresho, P. M. & Sani, R. L. 1987 On pressure boundary conditions for the incompressible Navier-Stokes equations. *Intl J. Numer. Meth. Fluids* **7**, 1111–1145.

Ho, C. M. & Huerre, P. 1984 Perturbed free shear layers. *Ann. Rev. Fluid Mech.* **16**, 365–424.

Hunt, J. C. R., Wray, A. A. & Moin, P. 1988 Eddies, streams and convergence zones in turbulent flows. *Center for Turbulence Research, Proc. Summer Program* 1988, p. 193.

Hussain, A. K. M. F. 1980 *Coherent Structures in Perturbed and Unperturbed Jets*. Lecture Notes in Physics, vol. 136, p. 252.

Hussain, A. K. M. F. & Zedan, M. F. 1978 Effects of the initial condition on the axisymmetric free shear layer: Effects of the initial momentum thickness. *Phys. Fluids* **21**, 1100–1112.

Hussain, A. K. M. F. & Zaman, K. M. B. Q. 1985 An experimental study of organized motions in the turbulent plane mixing layer. *J. Fluid Mech.* **159**, 85–104.

Kuethe, A. M. 1935 Investigation of the turbulent mixing regions formed by jets. *Trans. ASME: J. Appl. Mech.* **57**, A87–A95.

Lasheras, J. C. & Choi, H. 1988 Three-dimensional instability of a plane free shear layer: an experimental study of the formation and evolution of streamwise vortices. *J. Fluid Mech.* **189**, 53–86.

Liepmann, D. K. & Laufer, J. 1947 Investigations of free turbulent mixing. *NACA Tech. Note*. 1257.

Loucks, R. B. 1998 An experimental examination of the velocity and vorticity fields in a plane mixing layer. *PhD Dissertation*, University of Maryland.

Metha, R. D. & Westphal, R. V. 1986 Near-Field turbulence properties of single and two-stream plane mixing layers. *Exps. Fluids* **4**, 257–266.

Meneveau, C., Lund, T. S. & Cabot, W. H. 1996 A Lagrangian dynamic subgrid-scale model of turbulence. *J. Fluid Mech.* **319**, 353–385.

Moser, R. D., Rogers, M. M. & Ewing, D. W. 1998 Self-similarity of time-evolving plane wakes. *J. Fluid Mech.* **367**, 255–289.

Oster, D. & Wygnanski, I. 1982 The forced mixing layer between parallel streams. *J. Fluid Mech.* **123**, 91–130.

Townsend, A. A. 1976 *Structure of Turbulent Shear Flow*, 2nd Edn. Cambridge University Press.

Reichardt, H. 1942 Gesetzmassigkeitender freien turbulenz. *VDI-Forschungshung* **414**.

Riley, J. J. & Metcalfe R. W. 1980 Direct numerical simulation of a perturbed mixing layer. *AIAA Paper* 80-0274.

Robinson, S. K. 1991 The kinematics of turbulent boundary layer structure. *NASA TM*-103859.

Rogers, M. M. & Moser, R. D. 1992 The three-dimensional evolution of a plane mixing layer: the Kelvin-Helmholtz rollup. *J. Fluid Mech.* **243**, 183–226.

Rogers, M. M. & Moser, R. D. 1994 Direct simulation of a self-similar turbulent mixing layer. *Phys. Fluids* **6**, 903–923.

Sarghini, F., Piomelli, U. & Balaras, E. 1999 Scale-similar models for large-eddy simulations. *Phys. Fluids* **11**, 1596–1607.

Slessor, M. D., Bond, C. L. & Dimotakis, P. E. 1998 Turbulent shear-layer mixing at high Reynolds numbers: effects of inflow conditions. *J. Fluid Mech.* **376**, 115–138.

Spalart, P. R. 1988 Direct simulation of a turbulent boundary layer up to $R_\theta = 1410$. *J. Fluid Mech.* **187**, 61–98.

Vreman, B., Geurts, B. & Kuerten, H. 1997 Large-eddy simulation of the turbulent mixing layer. *J. Fluid Mech.* **339**, 357–390.

Weisbrot, I., Einav, S. & Wygnanski, I. 1982 The nonunique rate of spread of the two-dimensional mixing layer. *Phys. Fluids* **25**, 1691–1693/1100–1112.

Wygnanski, I. & Fiedler, H. E. 1970 The two-dimensional mixing region. *J. Fluid Mech.* **41**, 327–361.

Wygnanski, I., Champagne, F. & Marasli, B. 1986 On the large scale structures in two-dimensional, small-deficit, turbulent wakes. *J. Fluid Mech.* **168**, 31–71.